Solving the fully non-linear weakly dispersive Serre equations for flows over dry beds.

J.P.A. Pitt[a,*], C. Zoppou[a], S.G. Roberts[a]

[a]*Mathematical Sciences Institute, Australian National University, Canberra, ACT 0200, Australia*

Abstract

A numerical method for solving the Serre equations that can model flows over dry bathymetry is described. The method solves the Serre equations in conservation law form with a finite volume method. A finite element method is used to solve the auxiliary elliptic equation for the depth-averaged horizontal velocity. The numerical method is validated against the lake at rest analytic solution, demonstrating that it is well-balanced. The method is further validated and its convergence rate established using forced solutions containing the wetting and drying of bathymetry. The use of forced solutions extends previous validations performed for Serre equation solvers involving flows over dry bathymetry. Finally, the method is validated against experimental results for the run-up of a solitary wave on a sloped beach.

Keywords: Serre equations, dry bed

1. Introduction

Dispersion is an important phenomenon of waves in intermediate water depths; where the water depth is not much larger than the wavelengths of the waves. Our understanding of the effect of dispersion on water surface profiles is continually improving [1]. However, what is not well understood is the behaviour of these waves as they approach and inundate the coastline.

There is a family of wave equations that can be used to model the behaviour of dispersive waves as they inundate a dry bed [2]. The Serre equations [3] are an important member of this family of dispersive wave equations, as they do not make assumptions about the wave amplitude and thus are fully non-linear. For this reason they are considered the most appropriate model of dispersive waves as they approach and then inundate the coastline [2].

There are many numerical methods for solving the Serre equations that are capable of modelling flows over dry beds [4–7]. The most popular approach is to split the

*Corresponding author

Email addresses: jordan.pitt@anu.edu.au (J.P.A. Pitt), christopher.zoppou@anu.edu.au (C. Zoppou), stephen.roberts@anu.edu.au (S.G. Roberts)

Serre equations into their hyperbolic part given by the Shallow Water Wave Equations (SWWE) and their dispersive part [4, 6, 7]. These splitting schemes employ a modification to simulate wave-breaking; where only the SWWE are solved when some local wave breaking criteria is met.

Currently, there are no known analytic solutions to the Serre equations that include wetting and drying of a non-horizontal bed. Hence, numerical methods in the literature have relied on experimental results to demonstrate their validity when modelling inundation [4–7]. These validation tests are extended in this paper by using forced solutions of the Serre equations. Forced solutions allow the ability of the method to accurately solve problems containing the wetting and drying of bathymetry to be tested without relying on analytic solutions. Furthermore, to demonstrate the order of accuracy of the method for complicated problems a convergence analysis can be performed using forced solutions.

This paper also describes a new Finite Element Volume Method (FEVM) extension of the Finite Difference Volume Methods (FDVM) of Zoppou et al. [8]. In the FEVM a Finite Element Method (FEM) is used to solve the auxiliary elliptic equations instead of the finite difference methods used by the FDVM, leading to a more robust numerical method.

The Serre equations and their conservation properties are presented in the next section. Followed by a description of the FEVM. The numerical scheme will be validated against the lake at rest analytic solution, demonstrating that it is well-balanced. The method will then be validated for the wetting and drying of the bed using forced solutions to the Serre equations. Finally, the numerical method is validated against the experimental results of Synolakis [9] for the run-up of a solitary wave on a dry beach with a constant slope.

2. Serre Equations

The Serre equations are a system of partial differential equations that describe the free-surface waves of fluids whose motion is dominated by gravitational forces. The primitive variables of the Serre equations are the height of the free-surface $h(x,t)$ above the bed $b(x)$ and the depth-averaged horizontal velocity of a column of water $u(x,t)$. These variables are shown in Figure 1. The absolute location of the free surface is given by $w(x,t) = h(x,t) + b(x)$.

The Serre equations can be written in conservation law form with a source term [8]

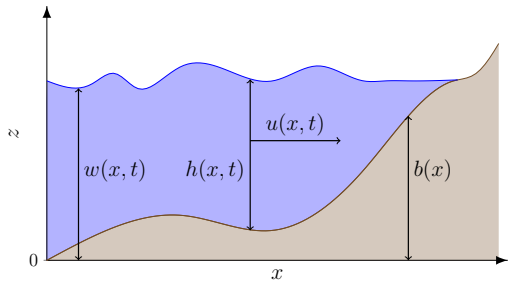

Figure 1: Diagram demonstrating a free surface flow ( ) over a bed ( ) where $w(x,t)$ is the absolute location of the free surface, $h(x,t)$ is the height of a column of fluid, $u(x,t)$ is the depth-averaged horizontal velocity of a column of fluid and $b(x)$ is the stationary bed profile.

as

$$\frac{\partial h}{\partial t} + \frac{\partial (uh)}{\partial x} = 0, \tag{1a}$$

$$\frac{\partial G}{\partial t} + \frac{\partial}{\partial x}\left(uG + \frac{gh^2}{2} - \frac{2h^3}{3}\left[\frac{\partial u}{\partial x}\right]^2 + h^2 u \frac{\partial u}{\partial x}\frac{\partial b}{\partial x}\right) + \underbrace{\frac{uh^2}{2}\frac{\partial u}{\partial x}\frac{\partial^2 b}{\partial x^2} - hu^2\frac{\partial b}{\partial x}\frac{\partial^2 b}{\partial x^2} + gh\frac{\partial b}{\partial x}}_{\text{source term}} = 0 \tag{1b}$$

with the conserved quantity

$$G = uh\left(1 + \frac{\partial h}{\partial x}\frac{\partial b}{\partial x} + \frac{h}{2}\frac{\partial^2 b}{\partial x^2} + \left[\frac{\partial b}{\partial x}\right]^2\right) - \frac{\partial}{\partial x}\left(\frac{h^3}{3}\frac{\partial u}{\partial x}\right). \tag{2}$$

2.1. Conservation Properties

Since the Serre equations can be written in conservation law form with a source term for h and G, these quantities should be conserved in a closed system, as long as the contribution of the source term is zero. Here conservation of a quantity q means that the total amount of q in a system occurring on the interval $[a,b]$ at time t

$$C_q(t) = \int_a^b q(x,t)\,dx$$

remains constant for all t. Additionally, the Serre equations conserve the momentum uh and the energy

$$\mathcal{H}(x,t) = \frac{1}{2}\left(gh\,(h+2b) + hu^2 + \frac{h^3}{3}\left[\frac{\partial u}{\partial x}\right]^2 + u^2 h\left[\frac{\partial b}{\partial x}\right]^2 - uh^2\frac{\partial u}{\partial x}\frac{\partial b}{\partial x}\right)$$

with $\mathcal{H}$ being a sum of the gravitational potential and kinetic energy throughout the depth of water. An equivalent set of equations in one-dimension was derived by Green and Naghdi [11] through conservation of the energy $\mathcal{H}$.

3. Description of Numerical Method

The Serre equations (1) are solved over a spatial domain that is partitioned into m cells $\left[x_{j-1/2}, x_{j+1/2}\right]$ of uniform length Δx. While time is discretised into time levels, t^n separated by a constant duration Δt.

Since the Serre equations can be written in conservation law form with a source term as follows

$$\frac{\partial \boldsymbol{Q}}{\partial t} + \frac{\partial F(\boldsymbol{Q})}{x} + S(\boldsymbol{Q}) = 0$$

with the conserved quantities $\boldsymbol{Q} = [h \;\; G]$, they can be solved using a Finite Volume Method (FVM) with a source term approximation. The finite volume formulation for the j^{th} cell is given by

$$\overline{\boldsymbol{Q}}_j^{n+1} = \overline{\boldsymbol{Q}}_j^n - \frac{\Delta t}{\Delta x}\left(F_{j+1/2}^n\left(\overline{\boldsymbol{Q}}^n\right) - F_{j-1/2}^n\left(\overline{\boldsymbol{Q}}^n\right)\right) + \Delta t S_j^n\left(\overline{\boldsymbol{Q}}^n\right) \tag{3}$$

which employs first-order forward Euler time integration. The term $\overline{\boldsymbol{Q}}_j^n$ is the average of the conserved quantities in the j^{th} cell at time t^n. The approximations to the flux across the right and left boundaries of the cell are $F_{j+1/2}^n\left(\overline{\boldsymbol{Q}}^n\right)$ and $F_{j-1/2}^n\left(\overline{\boldsymbol{Q}}^n\right)$ respectively and $S_j^n\left(\overline{\boldsymbol{Q}}^n\right)$ is the approximation to the source terms contribution to the cell from time t^n to t^{n+1}. Second-order accurate time stepping is achieved using a Strong Stability Preserving Runge-Kutta method [12] which employs a convex combination of (3).

To approximate the intercell fluxes $F_{j+1/2}^n\left(\overline{\boldsymbol{Q}}^n\right)$ and $F_{j-1/2}^n\left(\overline{\boldsymbol{Q}}^n\right)$ the method of Kurganov et al. [13] was used. While the source term is approximated with the well-balancing modifications proposed by Audusse et al. [14].

To achieve a second-order accurate method using (3), second-order accurate approximations to h, u, G, $\partial u/\partial x$, $\partial b/\partial x$, $\partial^2 b/\partial x^2$ inside a cell are required. The conserved quantities h and G are reconstructed from the cell averages, using a linear approximation to h and G over the cell. The bed, b is reconstructed using a cubic polynomial to ensure that the approximation to $\partial^2 b/\partial x^2$ in the source term (1) is second-order accurate.

The depth-averaged velocity u is obtained by solving (2) with a FEM given the reconstructions of h, G and b over the cell. Thus all the required approximations are obtained allowing the use of (3) to solve (1) producing the second-order scheme.

3.1. Flux Approximation

The method of Kurganov et al. [13] was employed because it can handle discontinuities across the cell boundaries and only requires an estimate of the maximum and minimum wave speeds, which are known for the Serre equations [8].

Only the calculation of the flux term $F_{j+1/2}^n\left(\overline{\boldsymbol{Q}}^n\right)$ is demonstrated as the process to calculate the flux term $F_{j-1/2}^n\left(\overline{\boldsymbol{Q}}^n\right)$ is identical but involves different cells. For a general quantity q the approximation of the flux term given by Kurganov et al. [13] is

$$F_{j+1/2}^n(q) = \frac{a_{j+1/2}^+ f\left(q_{j+1/2}^-\right) - a_{j+1/2}^- f\left(q_{j+1/2}^+\right)}{a_{j+1/2}^+ - a_{j+1/2}^-} + \frac{a_{j+1/2}^+ a_{j+1/2}^-}{a_{j+1/2}^+ - a_{j+1/2}^-}\left(q_{j+1/2}^+ - q_{j+1/2}^-\right) \tag{4}$$

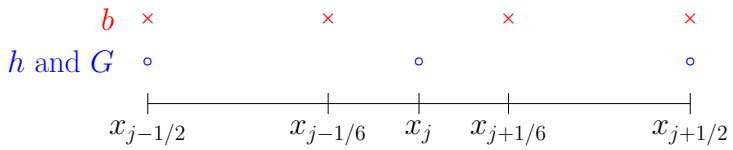

Figure 2: The conserved quantities h and G are reconstructed at $x_{j-1/2}$, x_j and $x_{j+1/2}$ (○) from their cell average values with a linear function over the cell. The bed, b is reconstructed at the equally spaced points $x_{j-1/2}$, $x_{j-1/6}$, $x_{j+1/6}$ and $x_{j+1/2}$ (×) from the nodal values with a cubic polynomial over the cell.

where $a^+_{j+1/2}$ and $a^-_{j+1/2}$ are given by bounds on the wave speed. With all the quantities on the right hand side representing their respective quantities at time t^n. Applying the wave speed bounds [8] then

$$a^-_{j+1/2} = \min\left\{0\ ,\ u^-_{j+1/2} - \sqrt{gh^-_{j+1/2}}\ ,\ u^+_{j+1/2} - \sqrt{gh^+_{j+1/2}}\right\}, \tag{5a}$$

$$a^+_{j+1/2} = \max\left\{0\ ,\ u^-_{j+1/2} + \sqrt{gh^-_{j+1/2}}\ ,\ u^+_{j+1/2} + \sqrt{gh^+_{j+1/2}}\right\}. \tag{5b}$$

The flux functions $f(q^-_{j+1/2})$ and $f(q^+_{j+1/2})$ across the cell edge $x_{j+1/2}$ are evaluated using the reconstructed values $q^-_{j+1/2}$ from the j^{th} cell and $q^+_{j+1/2}$ from the $(j+1)^{th}$ cell. For the continuity equation (1a)

$$f\left(h^\pm_{j+1/2}\right) = u^\pm_{j+1/2} h^\pm_{j+1/2} \tag{6}$$

and for G, (1b)

$$f\left(G^\pm_{j+1/2}\right) = u^\pm_{j+1/2} G^\pm_{j+1/2} + \frac{g}{2}\left(h^\pm_{j+1/2}\right)^2 - \frac{2}{3}\left(h^\pm_{j+1/2}\right)^3 \left[\left(\frac{\partial u}{\partial x}\right)^\pm_{j+1/2}\right]^2 + \left(h^\pm_{j+1/2}\right)^2 u^\pm_{j+1/2}\left(\frac{\partial u}{\partial x}\right)^\pm_{j+1/2}\left(\frac{\partial b}{\partial x}\right)^\pm_{j+1/2}. \tag{7}$$

The quantities $h^+_{j-1/2}$, $h^-_{j+1/2}$, $G^+_{j-1/2}$, $G^-_{j+1/2}$ and $(\partial b/\partial x)^\pm_{j+1/2}$ are given by the reconstructions. While $u^\pm_{j+1/2}$ and $(\partial u/\partial x)^\pm_{j+1/2}$ are obtained by the FEM.

3.2. Reconstruction

The quantities, h and G are reconstructed using piecewise linear functions over a cell generated from the neighbouring cell averages. While b is reconstructed from the nodal values of the neighbouring cells $j-2$, $j-1$, $j+1$ and $j+2$ using a cubic polynomial over those cells. The cubic polynomial ensures that the approximation to $\partial^2 b/\partial x^2$ is second-order accurate in cell j. The location of the reconstructed values of h, G and b are given in Figure 2, with their corresponding reconstruction functions being the polynomials that pass through their values at these locations. The bed is reconstructed at the cell edges and at $x_{j\pm1/6}$ as these locations are equally spaced within the cell.

3.2.1. The conserved quantities, h and G

Since h and G use the same reconstruction operators, the reconstruction operators will be described for a general quantity q. The values of q are reconstructed at $x_{j-1/2}$, x_j and $x_{j+1/2}$ from the cell averages $\overline{q}_j$ using the generalised minmod limiter [15]

$$q^+_{j-1/2} = \overline{q}^n_j - \frac{\Delta x}{2} d_j, \qquad q_j = \overline{q}^n_j, \qquad q^-_{j+1/2} = \overline{q}^n_j + \frac{\Delta x}{2} d_j \tag{8}$$

where

$$d_j = \text{minmod}\left(\theta \frac{\overline{q}^n_j - \overline{q}^n_{j-1}}{\Delta x}, \frac{\overline{q}^n_{j+1} - \overline{q}^n_{j-1}}{2\Delta x}, \theta \frac{\overline{q}^n_{j+1} - \overline{q}^n_j}{\Delta x}\right) \tag{9}$$

with $\theta \in [1, 2]$. Although h and G have three reconstruction locations in Figure 2, the resultant reconstructed function is a linear polynomial with the reconstructed nodal value at x_j being the average of the cell edge values.

3.2.2. Bed profile

The bed profile is reconstructed from the nodal values at the equally spaced locations $x_{j-1/2}$, $x_{j-1/6}$, $x_{j+1/6}$ and $x_{j+1/2}$ in the j^{th} cell shown in Figure 2. To do this an interpolating cubic polynomial for b over the j^{th} cell

$$C_j(x) = c_0 \left(x - x_j\right)^3 + c_1 \left(x - x_j\right)^2 + c_2 \left(x - x_j\right) + c_3$$

that passes through the adjacent cell nodal values x_{j-2}, x_{j-1}, x_{j+1} and x_{j+2} is used. This interpolating cubic has the coefficients

$$c_0 = \frac{-b_{j-2} + 2b_{j-1} - 2b_{j+1} + b_{j+2}}{12\Delta x^3}, \qquad c_1 = \frac{b_{j-2} - b_{j-1} - b_{j+1} + b_{j+2}}{6\Delta x^2},$$

$$c_2 = \frac{b_{j-2} - 8b_{j-1} + 8b_{j+1} - b_{j+2}}{12\Delta x}, \qquad c_3 = \frac{-b_{j-2} + 4b_{j-1} + 4b_{j+1} - b_{j+2}}{6}.$$

For the weak form of (2) to be valid, the bed profile must be continuous. To force a continuous bed profile the two possible values for b at the cell edges are averaged. Hence the reconstructions for b take the following values

$$b_{j\pm1/2} = \frac{1}{2}\left(C_j(x_{j\pm1/2}) + C_{j\pm1}(x_{j\pm1/2})\right), \qquad b_{j\pm1/6} = C_j(x_{j\pm1/6}). \tag{10}$$

From these reconstruction values the reconstructed cubic polynomial for the bed profile

$$P^b_j(x) = p^b_0(x - x_j)^3 + p^b_1(x - x_j)^2 + p^b_2(x - x_j) + p^b_3$$

passes through the values (10) and has the following coefficients

$$p^b_0 = \frac{-9b_{j-1/2} + 27b_{j-1/6} - 27b_{j+1/6} + 9b_{j+1/2}}{2\Delta x^3}, \quad p^b_1 = \frac{9b_{j-1/2} - 9b_{j-1/6} - 9b_{j+1/6} + 9b_{j+1/2}}{4\Delta x^2},$$

$$p^b_2 = \frac{b_{j-1/2} - 27b_{j-1/6} + 27b_{j+1/6} - b_{j+1/2}}{8\Delta x}, \qquad p^b_3 = \frac{-b_{j-1/2} + 9b_{j-1/6} + 9b_{j+1/6} - b_{j+1/2}}{16}.$$

The bed derivatives in (7) are approximated as follows

$$\left(\frac{\partial b}{\partial x}\right)^{-}_{j+1/2} = \frac{\partial}{\partial x} P^{b}_{j}(x_{j+1/2}), \qquad \left(\frac{\partial b}{\partial x}\right)^{+}_{j+1/2} = \frac{\partial}{\partial x} P^{b}_{j+1}(x_{j+1/2}). \tag{11}$$

3.3. Calculating u and $\partial u/\partial x$

To calculate u and $\partial u/\partial x$ a FEM is used to solve (2) for u given h, G and b. The FEM begins with the weak form of (2) using a test function v over the spatial domain Ω resulting in

$$\int_{\Omega} uh\left(1 + \left[\frac{\partial b}{\partial x}\right]^2\right) v - \frac{\partial}{\partial x}\left(\frac{1}{3}h^3\frac{\partial u}{\partial x}\right) v + uh\left(\frac{\partial h}{\partial x}\frac{\partial b}{\partial x} + \frac{1}{2}h\frac{\partial^2 b}{\partial x^2}\right) v \, dx = \int_{\Omega} Gv \, dx.$$

Integrating by parts with zero Dirichlet boundary conditions gives

$$\begin{aligned}\int_{\Omega} uh\left(1 + \left[\frac{\partial b}{\partial x}\right]^2\right) v \, dx + \int_{\Omega} \frac{1}{3}h^3\frac{\partial u}{\partial x}\frac{\partial v}{\partial x} \, dx \\ - \int_{\Omega} \frac{1}{2}uh^2\frac{\partial b}{\partial x}\frac{\partial v}{\partial x} \, dx - \int_{\Omega} \frac{1}{2}h^2\frac{\partial b}{\partial x}\frac{\partial u}{\partial x} v \, dx = \int_{\Omega} Gv \, dx.\end{aligned} \tag{12}$$

In the weak formulation a derivative on $h^3/3\,(\partial u/\partial x)$ is removed and the double derivative of the bed is reduced to a single derivative.

By assuming that time is fixed so that all the functions only vary in space, this formulation implies that by ensuring that G, h, b and $\partial b/\partial x$ have finite integrals over Ω, then u and $\partial u/\partial x$ must have finite integrals as well. To approximate the flux and the source terms in (1) requires $\partial u/\partial x$ to be well defined and thus have finite integrals. Therefore, it is assumed that at time t, h and G are square integrable functions and b is in the Sobolev space $\mathbb{H}^1(\Omega)$, where b and its first derivative are square integrable functions so that u is also a member of $\mathbb{H}^1(\Omega)$.

To approximate (12) the integration is performed over the cells and then summed together to obtain

$$\begin{aligned}\sum_{j=1}^{m}\Bigg(\int_{x_{j-1/2}}^{x_{j+1/2}} \Bigg[\Bigg(uh\left(1 + \left[\frac{\partial b}{\partial x}\right]^2\right) - \frac{1}{2}h^2\frac{\partial b}{\partial x}\frac{\partial u}{\partial x}\Bigg) v \\ + \left(\frac{1}{3}h^3\frac{\partial u}{\partial x} - \frac{1}{2}uh^2\frac{\partial b}{\partial x}\right)\frac{\partial v}{\partial x}\Bigg] dx\Bigg) = \sum_{j=1}^{m}\left(\int_{x_{j-1/2}}^{x_{j+1/2}} Gv \, dx\right)\end{aligned} \tag{13}$$

over the entire domain for all test functions v. The next step is to replace the functions for h, G, b, v and u with their corresponding basis function approximations.

For h and G the basis functions ψ are linear inside a cell and zero elsewhere, resulting in approximations that are square integrable, as required. For u and v the basis functions ϕ are quadratic inside the cell and continuous across the cell edges, therefore their approximations are in $\mathbb{H}^1(\Omega)$. The basis functions of u are quadratics to allow for a second-order approximation to $\partial u/\partial x$ in (7). Finally, for b the basis functions γ are

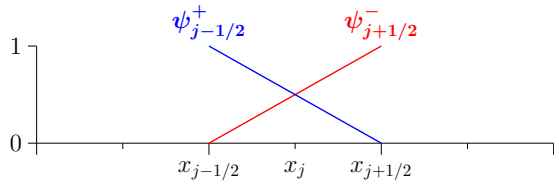

(a) ψ

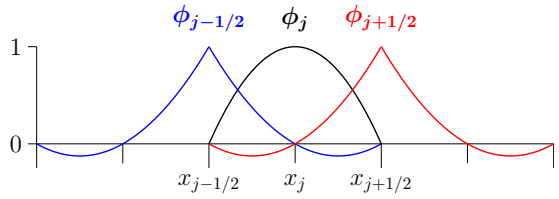

(b) ϕ

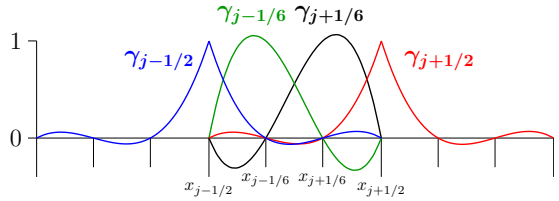

(c) γ

Figure 3: Support of the basis functions ψ, ϕ and γ which are non-zero over the j^{th} cell.

used, they are cubic polynomials inside the cell and continuous across the cell edges so that the approximation to b is in the appropriate function space. Cubic polynomials are used for b as a second-order approximation to $\partial^2 b/\partial x^2$ is required for the source term in (1). Examples of the basis functions ψ, ϕ and γ for the j^{th} cell are given in Figure 3, from which their equations can be derived.

The basis function approximation to h and G in the FEM written for a generic quantity q is

$$q = \sum_{j=1}^{m} \left(q^+_{j-1/2}\psi^+_{j-1/2} + q^-_{j+1/2}\psi^-_{j+1/2} \right) \tag{14a}$$

while for u it is

$$u = u_{1/2}\phi_{1/2} + \sum_{j=1}^{m} \left(u_j\phi_j + u_{j+1/2}\phi_{j+1/2} \right) \tag{14b}$$

and finally for b it is

$$b = b_{1/2}\gamma_{1/2} + \sum_{j=1}^{m} \left(b_{j-1/6}\gamma_{j-1/6} + b_{j+1/6}\gamma_{j+1/6} + b_{j+1/2}\gamma_{j+1/2} \right). \tag{14c}$$

Substituting all the functions in (13) with their corresponding basis function approximations (14) the integral equation becomes a matrix equation. Assembling these matrices results in

$$\mathbf{A}\hat{\boldsymbol{u}} = \boldsymbol{g} \tag{15}$$

where $\mathbf{A}$ is the stiffness matrix given by the integrals that contain u, $\hat{\boldsymbol{u}}$ is the vector containing the cell edge and nodal values of u and $\boldsymbol{g}$ is given by the integral of Gv. This is a penta-diagonal matrix equation which can be solved by direct banded matrix solution techniques such as those of Press et al. [16] to obtain $\hat{\boldsymbol{u}}$ and thus $u^{\pm}_{j+1/2}$ as desired. Note that $u^{\pm}_{j+1/2} = u_{j+1/2}$ since u is continuous across the cell edges.

To calculate $(\partial u/\partial x)^{\pm}_{j+1/2}$ the derivative of (14b) is taken. Since only $\phi_{j-1/2}$, ϕ_j and $\phi_{j+1/2}$ are non-zero over the j^{th} cell then

$$\left(\frac{\partial u}{\partial x}\right)^{-}_{j+1/2} = u_{j-1/2}\left.\frac{\partial \phi_{j-1/2}}{\partial x}\right|_{x_{j+1/2}} + u_j\left.\frac{\partial \phi_j}{\partial x}\right|_{x_{j+1/2}} + u_{j+1/2}\left.\frac{\partial \phi_{j+1/2}}{\partial x}\right|_{x_{j+1/2}}, \tag{16a}$$

$$\left(\frac{\partial u}{\partial x}\right)^{+}_{j+1/2} = u_{j+1/2}\left.\frac{\partial \phi_{j+1/2}}{\partial x}\right|_{x_{j+1/2}} + u_{j+1}\left.\frac{\partial \phi_{j+1}}{\partial x}\right|_{x_{j+1/2}} + u_{j+3/2}\left.\frac{\partial \phi_{j+3/2}}{\partial x}\right|_{x_{j+1/2}} \tag{16b}$$

where the subscript on the vertical line denotes that the derivatives of the basis functions ϕ are evaluated at $x_{j+1/2}$.

3.4. Source Term Approximation

To evolve the Serre equations using (3) requires an approximation to $S^n_j\left(\overline{\boldsymbol{Q}}^n\right)$. Equation (1a) has no source term, therefore only the calculation of the source term for equation (1b) is presented.

Since (3) is first-order accurate in time the source term approximation

$$S^n_j\left(\overline{\boldsymbol{Q}}^n_j\right) = -\frac{1}{2}\left(h^n_j\right)^2 u^n_j\left(\frac{\partial u}{\partial x}\right)^n_j\left(\frac{\partial^2 b}{\partial x^2}\right)^n_j + h^n_j\left(u^n_j\right)^2\left(\frac{\partial b}{\partial x}\right)^n_j\left(\frac{\partial^2 b}{\partial x^2}\right)^n_j - g h^n_j\left(\frac{\partial b}{\partial x}\right)^n_j \tag{17}$$

is sufficient. The quantities h^n_j and u^n_j are given by (8) and (15) respectively. To calculate the derivatives of b and u the approximations outlined in (11) and (14b) respectively are used to obtain

$$\left(\frac{\partial b}{\partial x}\right)_j = \frac{\partial}{\partial x}P^b_j(x_j) = p^b_2, \qquad \left(\frac{\partial^2 b}{\partial x^2}\right)_j = \frac{\partial^2}{\partial x^2}P^b_j(x_j) = 2p^b_3,$$

$$\left(\frac{\partial u}{\partial x}\right)_j = u_{j-1/2}\left.\frac{\partial \phi_{j-1/2}}{\partial x}\right|_{x_j} + u_j\left.\frac{\partial \phi_j}{\partial x}\right|_{x_j} + u_{j+1/2}\left.\frac{\partial \phi_{j+1/2}}{\partial x}\right|_{x_j}$$

Hence, all the approximations required to perform the FVM (3) are obtained, producing an approximation to (1) which is second-order accurate in space and first-order accurate in time.

3.5. Courant-Frederichs-Lewy Condition

To ensure the stability of the FVM (3) the Courant-Friedrichs-Lewy (CFL) condition [17] is used. The CFL condition is necessary for stability and ensures that time steps are small enough so that information is only transferred between neighbouring cells. For the Serre equations the CFL condition is

$$\Delta t \leq \frac{Cr}{\max_j \left\{a^{\pm}_{j+1/2}\right\}} \Delta x \tag{19}$$

where $a^{\pm}_{j+1/2}$ are the wave-speed bounds used in the flux approximation (5) and $0 \leq Cr \leq 1$ is the Courant number. Typically, the conservative $Cr = 0.5$ value is used in the numerical experiments.

3.6. Time-Stepping

To increase the order of accuracy in time the second-order SSP Runge-Kutta method [12] is employed, which is a convex combination of first-order forward Euler time steps (3) in the following way

$$\overline{\boldsymbol{Q}}^{(1)}_j = \overline{\boldsymbol{Q}}^n_j - \frac{\Delta t}{\Delta x}\left(F^n_{j+1/2}\left(\overline{\boldsymbol{Q}}^n_j\right) - F^n_{j-1/2}\left(\overline{\boldsymbol{Q}}^n_j\right)\right) + \Delta t S^n_j\left(\overline{\boldsymbol{Q}}^n_j\right), \tag{20a}$$

$$\overline{\boldsymbol{Q}}^{(2)}_j = \overline{\boldsymbol{Q}}^{(1)}_j - \frac{\Delta t}{\Delta x}\left(F^{(1)}_{j+1/2}\left(\overline{\boldsymbol{Q}}^{(1)}\right) - F^{(1)}_{j-1/2}\left(\overline{\boldsymbol{Q}}^{(1)}\right)\right) + \Delta t S^{(1)}_j\left(\overline{\boldsymbol{Q}}^{(1)}\right), \tag{20b}$$

$$\overline{\boldsymbol{Q}}^{n+1}_j = \frac{1}{2}\left(\overline{\boldsymbol{Q}}^n_j + \overline{\boldsymbol{Q}}^{(2)}_j\right). \tag{20c}$$

This results in a time stepping method that preserves the stability of the first-order method and is second-order accurate in time. Since all the spatial approximations are second-order accurate, the FEVM should be a second-order accurate solver for the Serre equations.

3.7. Well Balancing Modifications

To ensure that the method is well-balanced the work of Audusse et al. [14] is followed. This method was originally designed for the SWWE but was shown to apply equally well to the Serre equations [18].

The well balancing approach makes two changes to the method outlined above. The well-balancing modifications produce a different reconstruction of h which is used in the flux terms (6) and (7). Additionally, correction terms are added to the source term approximation (17). These changes ensure that the numerical approximations to the hydrostatic pressure term in the flux and the source term cancel for the lake at rest problem, where a still lake with a horizontal water surface remains stationary.

3.7.1. Modified Reconstruction of h

The modified reconstruction of h, $\bar{\bar{h}}$ depends on the reconstructions $w^{\pm}_{j+1/2}$ of w at the cell edge, which is calculated from its cell average values in the same way as h and G, (9). From these reconstructions the bed values

$$\tilde{b}^-_{j+1/2} = w^-_{j+1/2} - h^-_{j+1/2}, \qquad \tilde{b}^+_{j+1/2} = w^+_{j+1/2} - h^+_{j+1/2}$$

are calculated. Because $w^{\pm}_{j+1/2}$ and $h^{\pm}_{j+1/2}$ are discontinuous across the cell edges, $\tilde{b}^{\pm}_{j+1/2}$ may also be discontinuous across the cell edges unlike the previous reconstruction of the bed profile in (10). Given the maximum of these reconstructed bed values

$$\bar{\tilde{b}}_{j+1/2} = \max\left\{\tilde{b}^{-}_{j+1/2}, \tilde{b}^{+}_{j+1/2}\right\}$$

the reconstruction $\bar{\tilde{h}}$ at the cell edges is given by

$$\bar{\tilde{h}}^{-}_{j+1/2} = \max\left\{0, w^{-}_{j+1/2} - \bar{\tilde{b}}_{j+1/2}\right\}, \qquad \bar{\tilde{h}}^{+}_{j+1/2} = \max\left\{0, w^{+}_{j+1/2} - \bar{\tilde{b}}_{j+1/2}\right\}. \tag{21}$$

These reconstructions $\bar{\tilde{h}}^{\pm}_{j+1/2}$ replace $h^{\pm}_{j+1/2}$ in the flux terms (6) and (7).

3.7.2. Modified Source Term

The source term is modified by adding the corrective interface source terms $S^{-}_{j+1/2}\left(\overline{\boldsymbol{Q}}^{n}_{j}\right)$ and $S^{+}_{j-1/2}\left(\overline{\boldsymbol{Q}}^{n}_{j}\right)$ to obtain

$$S^{n}_{j}\left(\overline{\boldsymbol{Q}}^{n}_{j}\right) = \frac{1}{\Delta x} S^{-}_{j+1/2}\left(\overline{\boldsymbol{Q}}^{n}_{j}\right) + S_{ci}\left(\overline{\boldsymbol{Q}}^{n}_{j}\right) + \frac{1}{\Delta x} S^{+}_{j-1/2}\left(\overline{\boldsymbol{Q}}^{n}_{j}\right).$$

The term $S_{ci}\left(\overline{\boldsymbol{Q}}^{n}_{j}\right)$ is the source term approximation given in (17) with the approximation to $\partial b/\partial x$ altered to depend on $\tilde{b}^{\pm}_{j+1/2}$ like so

$$\left(\frac{\partial b}{\partial x}\right)_{j} = \frac{\tilde{b}^{-}_{j+1/2} - \tilde{b}^{+}_{j-1/2}}{\Delta x}.$$

The corrective interface source terms are calculated in the following way

$$S^{-}_{j+1/2}\left(\overline{\boldsymbol{Q}}^{n}_{j}\right) = \frac{g}{2}\left(\bar{\tilde{h}}^{-}_{j+1/2}\right)^{2} - \frac{g}{2}\left(h^{-}_{j+1/2}\right)^{2}, \quad S^{+}_{j-1/2}\left(\overline{\boldsymbol{Q}}^{n}_{j}\right) = \frac{g}{2}\left(h^{+}_{j-1/2}\right)^{2} - \frac{g}{2}\left(\bar{\tilde{h}}^{+}_{j-1/2}\right)^{2}.$$

These corrective terms ensure that when $u = 0$ and the water surface is horizontal, that $S^{n}_{j} = \left(F^{n}_{j+1/2} - F^{n}_{j-1/2}\right)/\Delta x$, ensuring that the method is well-balanced. The correction terms make use of $h^{\pm}_{j+1/2}$ obtained from the reconstruction (8) and the other reconstructions $\bar{\tilde{h}}^{\pm}_{j+1/2}$ from (21).

3.8. Dry Bed Handling Modifications

Dry beds present two issues for the FEM; (i) when h and G are small then small errors in h and G can produce large errors in u leading to instabilities and (ii) when $h = 0$ the stiffness matrix $\mathbf{A}$, (15) becomes singular.

Issue (i), where large errors in u are produced when h is small also arises when solving the SWWE due to $u = (uh)/h$ being undefined as uh and h vanish. For the Serre equations with horizontal beds, from (2) when $h \ll 1$

$$G = uh + O\left(h^{3}\right).$$

Since $h \ll 1$ the $O\left(h^{3}\right)$ terms can be neglected, and thus when h is small G is approximately equal to the momentum uh. Hence, the challenges posed by $h \to 0$ for

the SWWE and the Serre equations are similar. Therefore, dry bed handling techniques from the SWWE, such as the desingularisation transformations of Kurganov and Petrova [19] can be applied to the Serre equations.

These desingularisation transforms act by modifying the calculation of u given h and uh to avoid the singularity as the numerator and denominator approach zero, hence their name. The simplest such transformation is

$$u = \frac{(uh)h}{h^2 + \epsilon} \tag{22}$$

where ϵ is some small chosen parameter. The error introduced by this transformation is smallest when ϵ is smallest. However, as noted by Kurganov and Petrova [19] small values of ϵ lead to large numerical errors in the calculation of u. To avoid such errors ϵ can be made larger or following Kurganov and Petrova [19] a different desingularisation transformation can be employed. For the validations described later the simpler transformation with small values of ϵ was found to be more useful.

The desingularisation transformation for u, (22) produces an equivalent transformation of h

$$\frac{1}{h} \to \frac{h}{h^2 + \epsilon}. \tag{23}$$

Therefore, the reconstructed values of h in the FEM are transformed as follows

$$\frac{1}{h^{\pm}_{j-1/2}} = \frac{h^{\pm}_{j-1/2}}{\left(h^{\pm}_{j-1/2}\right)^2 + \epsilon} \tag{24}$$

where on the right hand side are the reconstructed values of h from (8) and the left hand side are the values of h used to defined the basis functions of the FEM (14a). In the numerical experiments in this paper, $\epsilon = 10^{-8}$. The transformation (24) is applied to all terms containing h in the FEM, avoiding the singularity as $h \to 0$.

To resolve issue (ii), where $\mathbf{A}$ becomes singular when h vanishes, (15) is solved for u in wet cells only. Wet and dry cells are identified using the cell average $\overline{h}$. A cell is considered dry when $\overline{h}_j \le h_{tol}$ and wet otherwise. For dry cells

$$\begin{aligned}
&h^+_{j-1/2} = 0, && G^+_{j-1/2} = 0, && w^+_{j-1/2} = b_{j-1/2},\\
&h_j = 0, && G_j = 0, && w_j = b_j,\\
&h^-_{j+1/2} = 0, && G^-_{j+1/2} = 0, && w^-_{j+1/2} = b_{j+1/2},\\
&u_j = 0
\end{aligned}$$

and if the neighbouring cells are dry then the velocity at the cell edges vanish so that

$$\begin{aligned}
u_{j-1/2} = 0 \quad &\text{when} \quad \overline{h}_{j-1} \le h_{tol},\\
u_{j+1/2} = 0 \quad &\text{when} \quad \overline{h}_{j+1} \le h_{tol}.
\end{aligned}$$

For the numerical experiments in this paper $h_{tol} = 10^{-12}$.

To ensure that the matrix solution of (15) is robust in the presence of small values of h, an LU decomposition with partial pivoting [16] is used. The pivot tolerance value for this matrix solution algorithm was $p_{tol} = 10^{-20}$ and any pivot values below p_{tol} were made equal to p_{tol}.

4. Validation

To confirm that the numerical method has the appropriate order of accuracy, is well-balanced and can handle dry-beds an analytic solution, forced solution and experimental results were used. Firstly, the convergence and conservation properties of the method for the lake at rest analytic solution are established. Secondly, the convergence rate of the numerical method is confirmed using a forced solution of the Serre equations. Finally, a numerical solution is compared to the experimental results of Synolakis [9], which involves a solitary wave travelling up a sloping beach.

4.1. Measures of Error

The L_2 vector norm was used to measure the error between a numerical solution at the cell nodes $\boldsymbol{q}^*$ and the analytic or forced solution at the cell nodes $\boldsymbol{q}$ using

$$L_2(\boldsymbol{q}, \boldsymbol{q}^*) = \begin{cases} \dfrac{\|\boldsymbol{q}^* - \boldsymbol{q}\|_2}{\|\boldsymbol{q}\|_2} & \|\boldsymbol{q}\|_2 > 0 \\ \\ \|\boldsymbol{q}^*\|_2 & \|\boldsymbol{q}\|_2 = 0. \end{cases}$$

By investigating the behaviour of $L_2(\boldsymbol{q}, \boldsymbol{q}^*)$ for numerical solutions with various Δx values the convergence rate of the method was established.

The conservation properties of the method are studied using the conservation error

$$C^*(\boldsymbol{q}, \boldsymbol{q}^*) = \begin{cases} \dfrac{|C^*(\boldsymbol{q}^*) - C^*(\boldsymbol{q})|}{|C^*(\boldsymbol{q})|} & |C^*(\boldsymbol{q})| > 0 \\ \\ |C^*(\boldsymbol{q}^*)| & |C^*(\boldsymbol{q})| = 0. \end{cases}$$

The conservation error $C^*(\boldsymbol{q}, \boldsymbol{q}^*)$ compares the total amount of q in the numerical solution at the end of the simulation $C^*(\boldsymbol{q}^*)$ to the total amount of q in the initial conditions $C^*(\boldsymbol{q})$. The total amount of a quantity is calculated numerically by summing the total amount of q in each cell. Fifth-order accurate Gaussian quadrature of a quartic interpolation of q, using the neighbouring nodal values is used to calculate the total amount of q in a cell.

4.2. Lake at Rest Solution Validation

The lake at rest is a stationary analytic solution of the Serre equations where a still lake has a horizontal water surface over any bathymetry. This solution is maintained due to the balance of the hydrostatic pressure and the forcing of the bed slope. A well-balanced numerical method should accurately reproduce this lake at rest stationary solution.

To test whether the method is well-balanced the following lake at rest solution

$$h(x,t) = \max\{a_0 - b(x), 0\}, \qquad b(x) = a_1 \sin(a_2 x),$$
$$u(x,t) = 0, \qquad G(x,t) = 0$$

was used. To demonstrate the capability of the method in the presence of dry and wet regions of the bed, the parameter values $a_0 = 0m$, $a_1 = 1m$ and $a_2 = 2\pi/50m^{-1}$

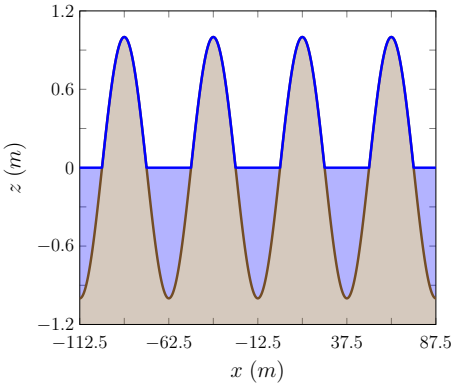

Figure 4: Numerical solution for w ( ) and b ( ) with $\Delta x = 100/2^{10}m$ for the lake at rest problem at $t = 10s$.

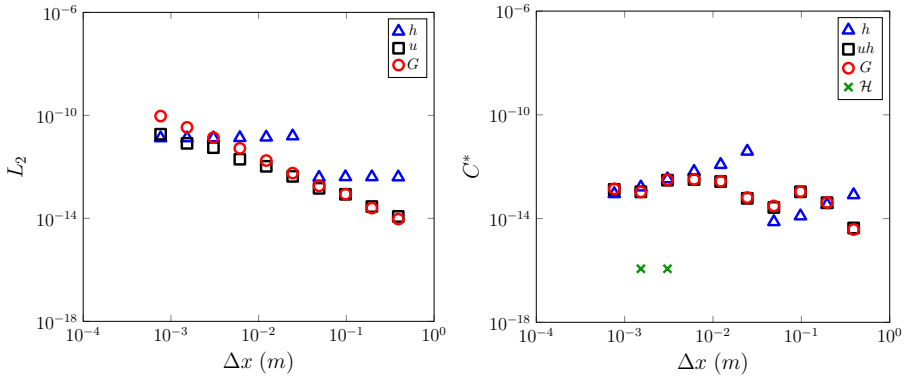

(a) Numerical Error (L_2)

(b) Conservation Error (C^*)

Figure 5: The numerical error (h, u and G) and conservation error (h, uh, G $\mathcal{H}$) against Δx for the lake at rest problem at $t = 10s$.

were chosen. These parameter values result in lakes with a horizontal free surface surrounded by dry regions.

For the numerical solutions the spatial domain was $x \in [-112.5m, 87.5m]$ and the final time was $t = 10s$, with the standard gravitational acceleration $g = 9.81m/s^2$. The spatial resolution of the method was varied so that $\Delta x = 100/2^k m$ with $k \in [8, \ldots, 17]$ and the CFL condition (19) was satisfied by having $\Delta t = Cr\Delta x/\sqrt{g}$ with condition number $Cr = 0.5$. The generalised limiter parameter $\theta = 1.2$ was used in (9). Dirichlet boundary conditions were used at both ends as the analytic solution is stationary.

The numerical method is assessed by comparing the numerical solution at $t = 10s$ to the analytic solution, which are the initial conditions.

An example numerical solution with $\Delta x = 100/2^{10}m \approx 0.0977m$ at $t = 10s$ is given in Figure 4. The numerical solution in this Figure is indistinguishable from the analytic solution at this scale and so the analytic solution has been omitted.

Examination of the L_2 errors depicted in Figure 5(a) reveals that the method repro-

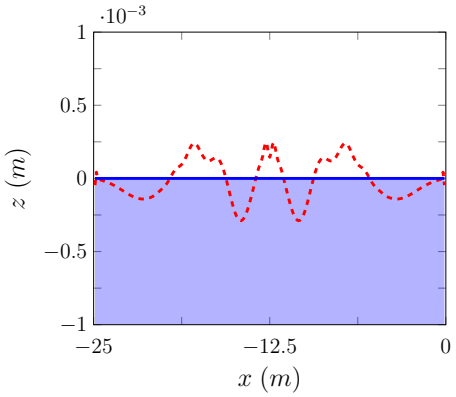

Figure 6: Numerical solution for w with (▭) and without (– –) well-balancing modifications over $[-25, 0]$ for the lake at rest problem at $t = 10s$ where $\Delta x = 100/2^{10}m$.

duced h, G and u precisely, accounting for round-off errors. The errors for h, G and u are increasing as $\Delta x \to 0$ due to an accumulation of the round-off errors.

The conservation errors as measured by C^* for h, uh, G and $\mathcal{H}$ are shown in Figure 5(b). The conservation error of these conserved quantities demonstrates that all quantities are conserved within machine precision, with $\mathcal{H}$ being conserved exactly for most numerical solutions, hence its disappearance from the log-log plot. The conservation error of $\mathcal{H}$ is small for the lake at rest solution since u and therefore the kinetic energy vanish.

These results demonstrate that the developed method has accurately reproduced the lake at rest solution and is therefore well-balanced. Without the employed well-balancing modifications the numerical solution quickly develops non-zero velocities and a non-horizontal water surface profile which can be seen in Figure 6.

4.3. Forced Solution Validation

There are currently no known analytic solution of the Serre equations for the wetting and drying of bathymetry. To test the capability of the numerical method in this environment a forced solution is used.

To generate a forced solution arbitrary functions for all of the primitive quantities; h, u and b, denoted $h^\#$, $u^\#$ and $b^\#$ respectively were selected. To ensure that these functions $h^\#$, $u^\#$ and $b^\#$ are exact solutions the Serre equations are modified by adding

the terms S_h and S_G to obtain the forced Serre equations

$$\frac{\partial h}{\partial t} + \frac{\partial (uh)}{\partial x} + S_h = 0,$$

$$\frac{\partial G}{\partial t} + \frac{\partial}{\partial x}\left(uG + \frac{gh^2}{2} - \frac{2h^3}{3}\left[\frac{\partial u}{\partial x}\right]^2 + h^2 u \frac{\partial u}{\partial x}\frac{\partial b}{\partial x}\right)$$

$$+\frac{uh^2}{2}\frac{\partial u}{\partial x}\frac{\partial^2 b}{\partial x^2} - hu^2\frac{\partial b}{\partial x}\frac{\partial^2 b}{\partial x^2} + gh\frac{\partial b}{\partial x} + S_G = 0$$

where

$$S_h = -\frac{\partial h^\#}{\partial t} - \frac{\partial (u^\# h^\#)}{\partial x},$$

$$S_G = -\frac{\partial G^\#}{\partial t} - \frac{\partial}{\partial x}\left(u^\# G^\# + \frac{g\left[h^\#\right]^2}{2} - \frac{2\left[h^\#\right]^3}{3}\left[\frac{\partial u^\#}{\partial x}\right]^2 + \left[h^\#\right]^2 u^\# \frac{\partial u^\#}{\partial x}\frac{\partial b^\#}{\partial x}\right)$$

$$-\frac{u^\#\left[h^\#\right]^2}{2}\frac{\partial u^\#}{\partial x}\frac{\partial^2 b^\#}{\partial x^2} + h^\#\left[u^\#\right]^2\frac{\partial b^\#}{\partial x}\frac{\partial^2 b^\#}{\partial x^2} - gh^\#\frac{\partial b^\#}{\partial x}.$$

These forced Serre equations are then numerically solved by solving the Serre equations (1) with the analytic values of S_h and S_G given $h^\#$, $u^\#$ and $b^\#$. Hence, the only error present in the numerical solutions of the forced Serre equations is the error produced by the numerical method used to solve the original Serre equations.

Note that since the choice of the forced solutions $h^\#$, $u^\#$ and $b^\#$ is arbitrary the solutions of the forced Serre equations need not be conservative or retain any properties of the underlying Serre equations.

4.3.1. Dry Bed Forced Solution Problem

To test the capability of the numerical method to solve the Serre equations the following expressions were chosen

$$h^\#(x,t) = a_0 \exp\left(-\frac{[(x - a_1 t) - a_2]^2}{2a_3}\right), \tag{25a}$$

$$u^\#(x,t) = a_4 \exp\left(-\frac{[(x - a_1 t) - a_2]^2}{2a_3}\right), \tag{25b}$$

$$b^\#(x) = a_5 \sin(a_6 x) \tag{25c}$$

for the primitive variables. These functions produce a Gaussian bump for h and u that travels at a fixed speed a_1 over a dry periodic bed. Thus, h and u will have constant

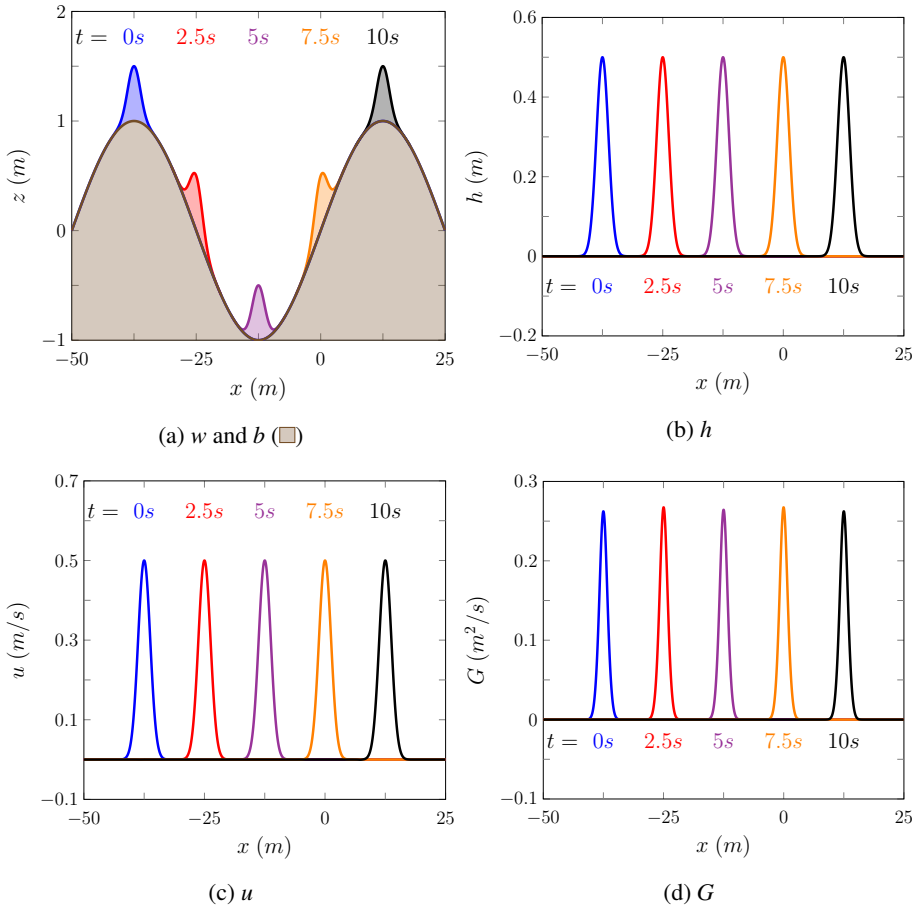

(a) w and b (▭)

(b) h

(c) u

(d) G

Figure 7: Example numerical solutions for w, b, h, G with $\Delta x = 100/2^{14}m$ at various times to the dry bed forced solution problem.

shape and travel in the positive x-direction over time. The quantity G will not maintain a constant shape due to its dependence on the bed slope which varies over x.

The values $a_0 = 0.5m$, $a_1 = 2\pi/(10a_7)\,m/s$, $a_2 = -3\pi/(2a_6)\,m$, $a_3 = \pi/(16a_6)m^2$, $a_4 = 0.5m/s$, $a_5 = 1.0m$ and $a_6 = \pi/25m^{-1}$ were used. These parameter values produce a Gaussian bump in h and u that has a width much smaller than the wavelength of the bed profile and travels precisely one wavelength of the bed in $10s$.

The domain of the numerical solutions was $x \in [-112.5m, 87.5m]$ with $t \in [0s, 10s]$. The standard gravitational acceleration $g = 9.81m/s^2$ was used. The spatial resolution of numerical methods was varied so that $\Delta x = 100/2^k m$ with $k \in [8, \ldots, 17]$. To satisfy the CFL condition (19) the temporal resolution $\Delta t = Cr\Delta x/\left(a_1 + a_4 + \sqrt{g\,(a_0)}\right)$ was chosen with condition number $Cr = 0.5$. The value $\theta = 1.2$ was used in the generalised minmod limiter (9) and Dirichlet boundary conditions were applied at the boundaries of the domain.

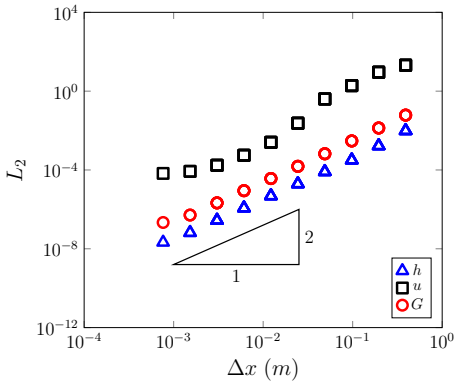

Figure 8: Errors as measured by L_2 against Δx for h, u, and G for the dry bed forced solution problem at $t = 10s$.

Plots of w, h, u and G are given in Figure 7 for the numerical solution with $\Delta x = 100/2^{14}m \approx 0.0061m$. The numerical solutions of w, h, u and G well reproduce their respective forced solutions.

The calculation of u in the presence of dry beds does possess significant errors due to the desingularisation transformation (24), as observed by the L_2 errors in Figure 8. For h and G the desired second-order accuracy is achieved for the entire range of Δx values. The velocity, u also attains second-order accuracy for Δx values around 10^{-2} however, the second-order accuracy is lost as Δx decreases further. This plateau in the error for small Δx values is due to the desingularisation techniques error in approximating h with (24) using $\epsilon = 10^{-8}$. When $h \approx 10^{-4}$ then $h^2 \approx \epsilon$ and the errors introduced by (24) become significant, hindering further reduction in the error of the velocity below 10^{-4}. To circumvent this requires lowering ϵ further which can significantly increase the error in the velocity [19]. Importantly, these errors in u are not transmitted to h and G as they occur when h is small and all the flux and source terms that include u are multiplied by some power of h.

The goal of using this forced solution was to confirm the convergence rate of the numerical method for the wetting and drying of variables beds. For this purpose the chosen desingularisation transform (24) with these ϵ and h_{tol} values was sufficient. These results demonstrate that the FEVM reproduced the forced solution well, validating the method for flows over dry bathymetry.

4.4. Run-up of a Solitary Wave

To study the run-up of incoming waves on linear beaches a series of experiments were conducted by Synolakis [9]. These experiments consisted of a number of run-up events for a wide array of breaking and non-breaking waves where snapshots of the entire water surface were taken at certain times. These experiments were all performed on the beach profile depicted in Figure 9, where all the quantities are non-dimensionalised [9]. A prime is used to denote that a quantity is non-dimensionalised. One of these experiments, which captured the run-up of a non-breaking solitary wave was used to assess the numerical method.

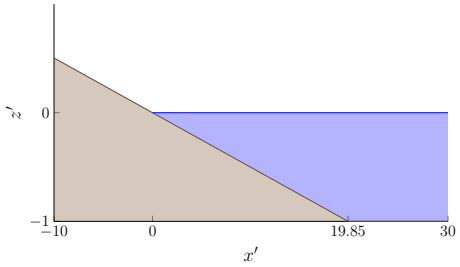

Figure 9: Diagram showing a longitudinal section of the wave tank for the run-up experiment with the water (■) and the bed (■) where the coordinates have been non-dimensionalised [9].

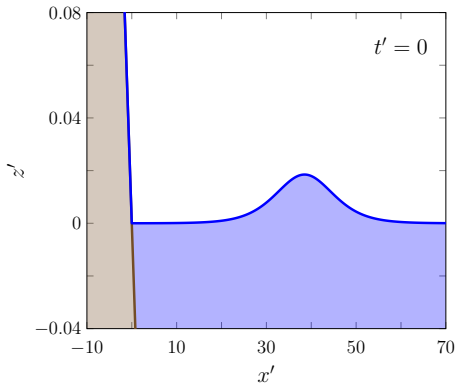

Figure 10: Initial water surface profile (■) over the bed (■) for the run-up experiment of Synolakis [9].

The numerical method used the non-dimensionalised quantities reported by Synolakis [9] to reproduce the experiment. The spatial domain was $x' \in [-30, 150]$ with a resolution of $\Delta x = 0.05$ and was run until $t' = 250$ with the CFL condition (19) satisfied by setting $\Delta t = 0.1\Delta x$. The spatial reconstruction used $\theta = 1.2$ and the acceleration due to gravity $g = 1$ was chosen to match the non-dimensionalisation.

The same initial conditions are used to construct this numerical experiment as those of Li et al. [5], producing the initial water surface profile depicted in Figure 10.

The non-dimensionalised water surface data is given at the various times in Figure 11. The error in conservation of h', $u'h'$, G' and $\mathcal{H}'$ by $t' = 250$ as measured by C^* are given in Table 1.

The numerical solution reproduces the incoming wave properties and the maximum run-up well, and compares well to numerical solutions presented in the literature [5, 6]. The experimental wave appears to be more skewed towards the shoreline, but this shape difference has all but disappeared as the wave begins to inundate the shore. The only other noticeable difference is that the numerical solution appears to receed further than the experimental results. The observed larger run-down is likely caused by the omission of bed friction for the Serre equations in this paper.

Both h' and $\mathcal{H}'$ are well conserved by the method throughout the run-up and run-down of the wave, particularly h'. The total energy $\mathcal{H}'$ of the method is also well conserved, however $\mathcal{H}'$ appears to have slightly increased in the method during the

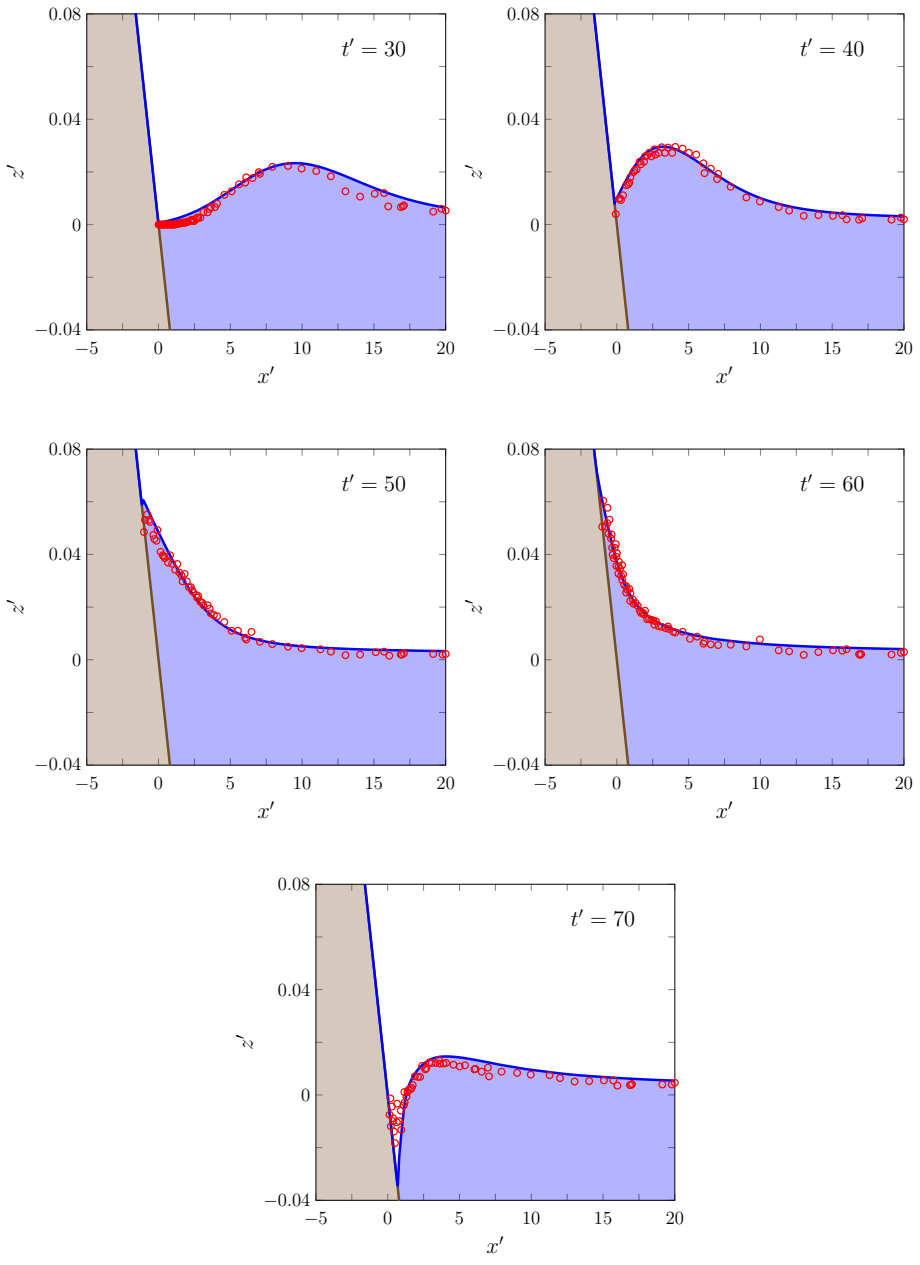

Figure 11: A comparison of the water surface profiles $w'(x', t')$ for the experiment (○) and the numerical solution (□) over the bed (□) at various times.

Quantity	$C^*\left(\boldsymbol{q}^0\right)$	$C^*\left(\boldsymbol{q}^*\right)$	$C^*\left(\boldsymbol{q}^0, \boldsymbol{q}^*\right)$
h'	2.40×10^2	2.40×10^2	1.33×10^{-10}
$u'h'$	-3.19×10^{-2}	3.19×10^{-2}	4.96×10^{-4}
G'	-3.19×10^{-2}	3.19×10^{-2}	5.88×10^{-4}
$\mathcal{H}'$	-1.18×10^2	-1.18×10^2	3.77×10^{-7}

Table 1: Initial and final ($t' = 250$) total amounts and the conservation error for the conserved quantities in the numerical solution of the run-up experiment. Here the absolute value of the total amount of uh and G are taken in the error as the wave has reflected off the beach.

run-up process due to the handling of the dry bed problem. During this experiment kinetic energy is converted into gravitational potential energy and then back again as the wave is reflected. By $t' = 250$ the reflection of the wave is complete and the total amount of $u'h'$ and G' have changed signs, although their errors are small if this is considered. Given that kinetic energy and gravitational energy were exchanged and the handling of the dry bed, the conservation error of $u'h'$ and G' is good.

The Serre equations have reproduced the experimental result of Synolakis [9] well, experimentally validating the numerical methods ability to solve the Serre equations for flows over dry beds.

5. Conclusion

A second-order numerical method for the one-dimensional Serre equations with varying bathymetry was described. The method uses a FVM to solve the Serre equations in conservation law form and improves previous versions of the FVM solvers for the Serre equations [8], by using a FEM to solve for the depth-averaged horizontal velocity. The method is modified to ensure that it is well-balanced, maintaining a steady state solution over arbitrary bathymetry and is able to handle flows over dry beds. The numerical method was validated against the lake at rest stationary solution and shown to be well-balanced. Furthermore, it reproduced forced solutions containing the wetting and drying of variable beds with second-order accuracy, affirming its ability to adequately solve the Serre equations for flows over dry beds. Finally, the numerical solution was compared to the experimental results of Synolakis [9], demonstrating the ability of the numerical method to accurately reproduce physical results involving wave run-up on a dry bed. These validation results extend those produced by other solvers of the Serre equations for flows over dry beds [4–7] by demonstrating convergence using forced solutions.

References

[1] J.P.A. Pitt, C. Zoppou, and S.G. Roberts. Behaviour of the Serre equations in the presence of steep gradients revisited. *Wave Motion*, 76(1):61–77, 2018.

[2] D. Lannes and P. Bonneton. Derivation of asymptotic two-dimensional time-dependent equations for surface water wave propagation. *Physics of Fluids*, 21 (1):16601, 2009.

[3] F. Serre. Contribtion à l'étude des écoulements permanents et variables dans les canaux. *La Houille Blanche*, 6:830–872, 1953.

[4] M. Tissier, P. Bonneton, F. Marche, F. Chazel, and D. Lannes. Serre Green-Naghdi modelling of wave transformation breaking and run-up using a high-order finite-volume finite-difference scheme. *Coastal Engineering Proceedings*, 1(32): 1–13, 2011.

[5] M. Li, P. Guyenne, F. Li, and L. Xu. High order well-balanced CDG-FE methods for shallow water waves by a Green-Naghdi model. *Journal of Computational Physics*, 257(1):169–192, 2014.

[6] A. G. Filippini, M. Kazolea, and M. Ricchiuto. A flexible genuinely nonlinear approach for nonlinear wave propagation, breaking and run-up. *Journal of Computational Physics*, 310:381–417, 2016.

[7] J.S.A. do Carmo, J.A. Ferreira, and L. Pinto. On the accurate simulation of nearshore and dam break problems involving dispersive breaking waves. *Wave Motion*, 85:125 – 143, 2019.

[8] C. Zoppou, J. Pitt, and S. Roberts. Numerical solution of the fully non-linear weakly dispersive Serre equations for steep gradient flows. *Applied Mathematical Modelling*, 48:70–95, 2017.

[9] C.E. Synolakis. The runup of solitary waves. *Journal of Fluid Mechanics*, 185: 523–545, 1987.

[10] F.J. Seabra-Santos, D.P. Renouard, and A.M. Temperville. Numerical and experimental study of the transformation of a solitary wave over a shelf or isolated obstacle. *Journal of Fluid Mechanics*, 176:117–134, 1981.

[11] A.E. Green and P.M. Naghdi. A derivation of equations for wave propagation in water of variable depth. *Journal of Fluid Mechanics*, 78(2):237–246, 1976.

[12] S. Gottlieb, C. Shu, and E. Tadmor. Strong stability-preserving high-order time discretization methods. *Review, Society for Industrial and Applied Mathematics*, 43(1):89–112, 2001.

[13] A. Kurganov, S. Noelle, and G. Petrova. Semidiscrete central-upwind schemes for hyperbolic conservation laws and Hamilton-Jacobi equations. *Journal of Scientific Computing, Society for Industrial and Applied Mathematics*, 23(3):707–740, 2002.

[14] E. Audusse, F. Bouchut, M. Bristeau, R. Klein, and B. Perthame. A fast and stable well–balanced scheme with hydrostatic reconstruction for shallow water flows. *Journal of Scientific Computing, Society for Industrial and Applied Mathematics*, 25(6):2050–2065, 2004.

[15] B. Van Leer. Towards the ultimate conservative difference scheme. IV. A second-order sequel to Godunov's method. *Journal of Computational Physics*, 32(1): 101–136, 1979.

[16] W.H. Press, S.A. Teukolsky, W.T. Vetterling, and B.P. Flannery. *Numerical Recipes in C*. Cambridge University Press, London, 2nd edition, 2002.

[17] R. Courant, K. Friedrichs, and H. Lewy. On the partial difference equations of mathematical physics. *IBM Journal of Research and Development*, 11(2):215–234, 1967.

[18] J. Pitt. *A Second Order Well Balanced Hybrid Finite Volume and Finite Difference Method for the Serre Equations*. Honour's thesis, Australian National University, Mathematical Sciences Institute, College of Physical and Mathematical Sciences, Australian National University, Canberra, ACT 2600, Australia, 2014.

[19] A. Kurganov and G. Petrova. A second-order well-balanced positivity preserving central-upwind scheme for the Saint-Venant system. *Communications in Mathematical Sciences*, 5(1):133–160, 2007.